ResearchGate

See discussions, stats, and author profiles for this publication at: https://www.researchgate.net/publication/231649833

Redox pathways for HCOOH decomposition over CeO2 surfaces

ARTICLE *in* THE JOURNAL OF PHYSICAL CHEMISTRY C · JUNE 2008

Impact Factor: 4.77 · DOI: 10.1021/jp8016425

CITATIONS
65

READS
30

2 AUTHORS:

Sanjaya D. Senanayake
Brookhaven National Laboratory
109 PUBLICATIONS **1,794** CITATIONS
SEE PROFILE

David Mullins
Oak Ridge National Laboratory
139 PUBLICATIONS **3,932** CITATIONS
SEE PROFILE

Available from: Sanjaya D. Senanayake
Retrieved on: 01 February 2016

Redox Pathways for HCOOH Decomposition over CeO_2 Surfaces

Sanjaya D. Senanayake and David R. Mullins*

Oak Ridge National Laboratory, P.O. Box 2008, MS 6201, Oak Ridge, Tennessee 37831-6201

Received: February 25, 2008; Revised Manuscript Received: April 22, 2008

The reaction of HCOOH, the simplest C-1 carboxylic acid, has been studied on oxidized (CeO_2) and reduced cerium oxide (CeO_X) thin films. HCOOH has been proposed as an important C1 precursor to the formation of CO_2 and H_2 in the water-gas-shift (WGS) reaction, in which ceria is also used as a stable support rich in oxygen. The HCOOH is observed to adsorb by way of a formate intermediate species ($HCOO^-$) through the dissociation of the acidic H over both CeO_2 (Ce^{4+}) and CeO_X (Ce^{4+}/Ce^{3+}) surfaces. On the fully oxidized CeO_2 surface, this H species reacts with surface O and desorbs as H_2O when the temperature is <300 K. In addition to water, temperature programmed desorption spectra indicate the evolution of CO_2 and H_2 between 350 and 400 K followed by CO desorption in two regimes at 450 and 525 K. On reduced ceria, only CO and H_2 were produced between 450 and 600 K. The reaction of HCOOH with ceria therefore leads to both the reduction of the oxide, through the formation of H_2O and CO_2, and oxidation of the oxide, through decomposition to H_2 and CO, depending on the initial state of the ceria. C K-edge near-edge X-ray absorption fine structure and soft X-ray photoelectron spectroscopy indicate that formate and −OH were the only surface intermediates.

1. Introduction

Formic acid is the simplest molecule with a carboxylic acid functional group and is a very important intermediate in many industrial chemical processes. One such process is the 'water-gas-shift' (WGS) reaction (reaction 1). The formation of hydrogen by WGS has been promoted as a potential route for producing this critical alternative fuel. In WGS, the formation of formic acid/formates from CO and H_2O has been proposed as a rate-determining step in the reaction.[1] Cerium oxide, generally supporting noble metal particles, has been identified as an excellent heterogeneous catalyst in this reaction.[2] Ceria's well-known oxygen storage capacity is believed to promote the reaction extensively.[3]

$$CO + H_2O \leftrightarrow HCOOH \leftrightarrow CO_2 + H_2 \qquad (1)$$

Several studies have addressed the production of CO_2 and H_2 via a formate intermediate over Pt/CeO_2[4] and Au/CeO_2[5,6] under ambient catalytic conditions. Jacobs et al. identified a critical interaction between reduced ceria and the Pt metal in decomposing the resulting bidentate formate species.[4] They state that the C−H bond breaking of the adsorbate is likely to be the rate-limiting step for the water-assisted decomposition of formic acid. Haruta et al. assert that Au/CeO_2 is much more active and selective than the Pt/CeO_2 catalyst.[6] In their study, CO_2 was produced at 100% conversion up to 623 K.[6] The study further states that the reducibility of the cerium oxide substrate promotes the reaction compared to other oxide systems such as Au/TiO_2.

Attention has also been given to the reverse water gas shift process, where the conversion of CO_2 exhaust produces HCOOH and CO feedstocks.[7] In light of the environmental implications resulting from CO_2 emissions, this manner of CO_2 sequestration and its use as a sustainable fuel source is novel and has been considered promising.

On many oxide surfaces, formic acid rapidly deprotonates through the loss of the acidic H to produce an adsorbed formate intermediate. This critical first step is also expected for the reactions of higher order carboxylic acids (>C1).[8] The adsorbed intermediates may then further react to produce CO_2 and H_2 by dehydrogenation (reaction 2) or CO and H_2O by dehydration (reaction 3). Competing with these pathways is the recombination of the formate ($HCOO^-$) intermediate with surface H. On reducible oxides the adsorbed H species may be consumed through a reaction with surface O (or OH) to thereby release H_2O instead of formic acid. This will then promote the forward reaction toward the formation of CO or CO_2.

The present model for metal oxide selectivity toward dehydrogenation or dehydration of HCOOH is related to the acidity/basicity of the oxide surface.[8] Basic oxide surfaces favor the dehydrogenation pathway (2) and the acidic surfaces tend toward the dehydration pathway (3). The presence of defects and the reducibility of the oxide are also thought to effect the CO/CO_2 ratio.[8]

$$HCOOH(g) \leftrightarrow HCOO^-(a) + H(a) \leftrightarrow CO_2(g) + H_2(g) \quad \text{dehydrogenation} \qquad (2)$$

$$HCOOH(g) \leftrightarrow HCOO^-(a) + H(a) \rightarrow CO(g) + H_2(g) \quad \text{dehydration} \qquad (3)$$

$$HCOOH(g) \rightarrow HCOO^-(a) + H(a) + V_O \rightarrow H_2CO(g) + O(a) \qquad (4)$$

The reduction of formate to formaldyde (H_2CO) (reaction 4),[9,10] ketonization reactions,[11] and dehydration to form ketene[12] have also been observed on oxide surfaces and are readily promoted over reducible surfaces.

The most studied of model systems are the TiO_2 surfaces, where the adsorption and reaction has been thoroughly reviewed.[13] To summarize, HCOOH adsorbs molecularly onto

* Corresponding author. Phone: 865-574-2796. Fax: 865-576-5235. E-mail: mullinsdr@ornl.gov.

10.1021/jp8016425 CCC: $40.75 © 2008 American Chemical Society
Published on Web 06/11/2008

rutile TiO_2 at low temperature (~100 K) but desorbs by ~200 K, leaving formate ($HCOO^-$) and surface hydroxyl species. The stable formate species on the (110) surface has a bridging bidentate adsorption geometry (O−C−O angle at 126°) with the O atoms bonded to two Ti cations.[14] A minor contribution of a chelating bidentate species, with both O atoms bound to a single Ti cation, has also been observed.[15] TiO_2 exhibits both dehydrogenation (<500 K) and dehydration (>500 K) decomposition pathways. Desorption of H_2CO and traces of C_2H_2 are also seen from defected surfaces.

ZnO, a wurtzite structured material, offers (0001) and (000$\bar{1}$) surfaces with polar Zn and O terminations, respectively. When the ZnO(000$\bar{1}$)-O-terminated surface is exposed to HCOOH, multilayers are seen at 110 K.[14] At 340 K, the formate is the sole adsorbate. The formate was identified by its characteristic π^* resonance at 288.7 eV in the C K-edge near-edge X-ray absorption fine structure (NEXAFS). This resonance is clearly distinguishable from those of carbonates (CO_3^{2-}) and carbonyl (CO), which have resonances at 290.5 and 287.9 eV, respectively. The O-terminated surface is largely unreactive and the formate adopts a monodentate configuration that is reported to be tilted at 55° with respect to surface normal. On the metallic-like ZnO(0001)-Zn surface, no preferred orientation is reported;[16] however, this surface is more reactive, decomposing the formate at >575 K to yield CO, CO_2, H_2, and H_2O with a selectivity favoring the dehydrogenation pathway.

The reactions of HCOOH over a CeO_2 (001) film and CeO_2 (111) single crystal surfaces have been reported by Stubenrauch et al.[17] In this work, they identified the formation of monodentate formate and hydroxyl species using high-resolution electron energy loss spectroscopy (HREELS). On both surfaces, decomposition occurs above 600 K. The dehydration pathway (reaction 3) is favored on the basis of the CO/CO_2 ratio. They also report the formation of a small amount of H_2CO from the formate decomposition. Another fluorite-type surface, $UO_2(111)$,[18] showed two distinct pathways for dehydration/dehydrogenation from formate, with decomposition with dehydration ($CO + H_2O$) favored over the oxidized surface and dehydrogenation ($CO_2 + H_2$) favored over the reduced surface. H_2CO was also reported in considerable quantities arising from the reductive coupling of the adsorbate to surface defects.

In addition to understanding the adsorption and decomposition of formic acid on the reducible cerium oxide surface, another motivation of this study is to compare the reactivity of HCOOH to other C1 oxygenated molecules. The adsorption and reaction of methanol and formaldehyde are especially relevant to this study as these contain isolated alcohol and aldehyde functional groups, respectively, whereas formic acid presents both of these functionalities simultaneously. Methanol adsorbs on ceria via a methoxy species (CH_3O-) that is accompanied by the formation of hydroxy (−OH) on the oxide.[19] CeO_2 is reduced through the desorption of H_2O at 200 K and formaldehyde at ~550 K. With the introduction of O vacancies (V_O) and Ce^{3+} on CeO_X, water formation is suppressed and the methoxy and hydroxyl intermediates further decompose to yield CO and H_2 at 640 K. Formaldehyde (H_2CO) adsorbs on the oxidized surface by way of a dioxymethylene intermediate (H_2CO_2).[20] On oxidized CeO_2, this intermediate does not dissociate and desorbs as formaldehyde between 200 and 400 K. The presence of Ce^{3+} and O vacancies creates a strongly bound dioxymethylene species that further reacts to form formate (HCO_2) and methoxy intermediates that decompose to produce H_2, CO, and H_2CO above 400 K.

On oxidized $CeO_2(111)$, the adsorption of formic acid appears to be analogous to that of methanol, losing the acidic proton and strongly binding to the ceria as a formate. This process is largely irreversible and the formate goes on to decompose into various dehydrogenated products, as does methoxy. On a reduced surface, all three molecules undergo similar fates, primarily decomposing into CO and H_2. Formic acid is unique in that C−O bond cleavage occurs, which oxidizes the ceria substrate.

2. Experimental Section

This work was performed in two different ultrahigh vacuum (UHV) chambers. Soft X-ray photoelectron spectroscopy (sXPS) and NEXAFS data were collected using synchrotron radiation at the National Synchrotron Light Source (NSLS) on beam line U12a. The temperature programmed desorption (TPD) experiments were undertaken at Oak Ridge National Laboratory (ORNL). The specifics of the UHV chambers and the design of experimental setups for the systems at Oak Ridge[21] and at the NSLS[19] have been described previously.

The recipe for the preparation of ceria thin films has also been presented previously.[22] The surfaces were grown in situ by evaporation of Ce metal in an O_2 environment (CeO_2, 1×10^{-7} Torr; CeO_X, 8×10^{-9} Torr) on to a hot (700 K) Ru(0001) substrate. The growth of labeled $Ce^{18}O_2$ and $Ce^{18}O_X$ was performed by substituting isotopically labeled $^{18}O_2$ (>95% isotopic purity, Cambridge Isotopes) instead of $^{16}O_2$. A homemade evaporator was used at ORNL and an Omicron EFM 3 was used at the NSLS. The order of these films was checked using low-energy electron diffraction (LEED). A hexagonal p(1.4×1.4) pattern, relative to the Ru(0001) (1×1) pattern, was attributed to $CeO_X(111)$.

The formic acid (Sigma-Aldrich, reagent grade) was purified by several freeze−pump−thaw cycles and checked by mass spectrometry prior to the experiments. The adsorbate was introduced onto the sample at the NSLS by way of a high-precision leak valve attached to the UHV chamber using a "back-filling" technique. Saturation coverage was achieved following an exposure of ca. 1 L (1×10^{-6} Torr s). For experiments performed at ORNL, the HCOOH was introduced using an effusive gas doser.[21]

C K-edge NEXAFS data were obtained using a partial yield electron detector with a grid bias set at −225 eV. The photon energy resolution was ca. 0.5 eV and the angle of incidence was 0° and 65° with respect to the sample normal. The photon energy was calibrated using the dip in the photon flux at 284.7 eV.[23] Contributions from higher order Ce M_{IV} and M_V features appeared at apparent photon energies of ca. 295 and 301.5 eV, respectively.[24] These features were removed by subtracting spectra obtained with the grid biased to −320 eV, which only passed electrons excited by higher order radiation. Finally, the spectra with adsorbates were normalized to spectra recorded without adsorbates.

The XPS data were collected using a VSW 125 hemispherical analyzer with the sample oriented such that the photon incident angle was 35° and electron emission angle was 30° relative to the surface normal. The photon energies used for C 1s and O 1s were 400 and 600 eV, respectively. The instrumental resolution was ca. 0.5 eV. The binding energy was calibrated relative to the Ce 4d satellite feature at 122.3 eV.[19]

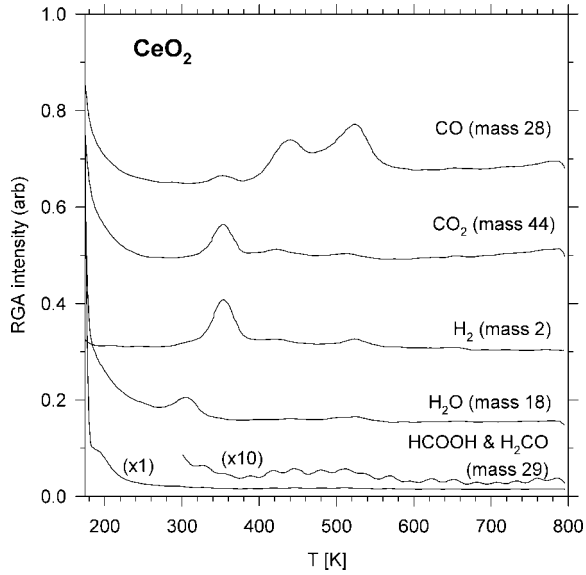

Figure 1. Temperature programmed desorption from HCOOH adsorbed on $CeO_2(111)$ at 100 K.

TPD experiments were performed at ORNL with a sample bias of −70 V to prevent electron stimulated reactions induced by the mass spectrometer ionizer. The temperature was ramped at 2 K/s.

The Ce oxidation state was determined using the Ce 4d features at the NSLS and the Ce 3d features at ORNL. The accuracy of the Ce^{4+}/Ce^{3+} content is estimated to be ±0.10, for example $CeO_{1.75\pm0.05}$.

3. Results

3.1. Stoichiometric CeO_2 Surface. ***3.1.1. Temperature Programmed Desoprtion.*** Figure 1 shows the TPD following HCOOH adsorption onto fully oxidized CeO_2 at 100 K. H_2 (mass 2), H_2O (mass 18), CO (mass 28), CO_2 (mass 44), and HCOOH (mass 29) were the most prominent desorption products. A trace amount of H_2CO was observed [mass 29 (×10) in Figure 1]. Mass 29 was monitored because it is the strongest cracking fragment for both HCOOH and H_2CO. A comparison between mass 46 and mass 29 indicated that the mass 29 desorption at below 300 K was due to HCOOH and the weak desorption above 400 K was due to H_2CO. Desorption occurring below 200 K in the mass 18, 28, and 44 spectra was attributed to artifacts produced by HCOOH on the basis of comparison between these masses and the desorption at mass 29 and 46.

Physisorbed HCOOH desorbs at ca. 160 K. This feature dominated the TPD spectra shown in Figure 1, so the spectra have been cut off at 175 K in order to focus on the reaction products. More strongly adsorbed HCOOH was evident at 200 K with a tail extending to 300 K. H_2O was observed at 300 K. This temperature was significantly higher than the water desorption at ca. 200 K that occurred following the adsorption of either CH_3OH[19] or H_2O[21] on oxidized ceria. At 355 K, H_2 and CO_2 desorb simultaneously, indicating a dehydrogenation of the surface intermediate. Two intense CO desorption peaks were evident at 440 and 520 K. Weak H_2, H_2O, H_2CO, and CO_2 desorption can be observed in this range as well.

A quantitative estimate of the amount of CO_2 and CO produced was obtained by adsorbing HCOOH on clean Ru(0001). Sun and Weinberg[25] reported that the chemisorbed

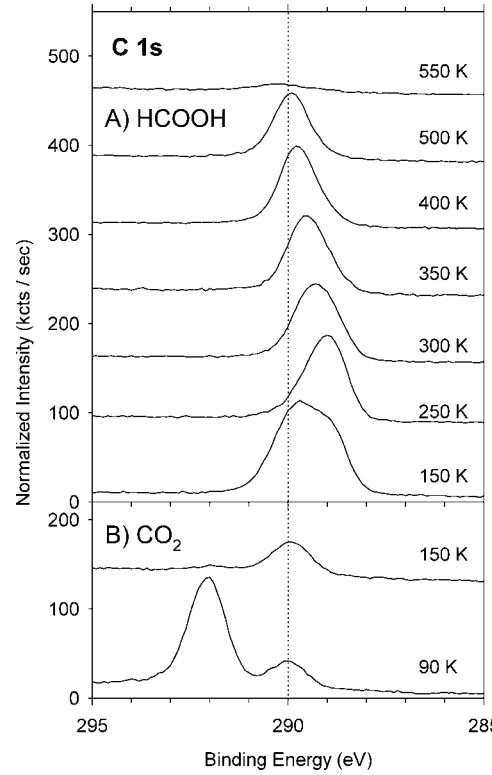

Figure 2. C 1s sXPS following (a) HCOOH and (b) CO_2 adsorption on $CeO_2(111)$ at 90 K and then annealed as indicated.

HCOOH coverage on Ru(0001) was 5.2 nm^{-2}. This then decomposed to produce 2.5 CO nm^{-2} and 2.7 CO nm^{-2}. The integrated CO_2 and CO intensities from $CeO_2(111)$ in Figure 1, compared to the integrated intensities from Ru(0001), indicate the amount of CO_2 and CO produced was 1.6 and 2.3 nm^{-2}, respectively. The total, 3.9 nm^{-2}, is ca. 0.5 ML relative to the O or Ce densities on the $CeO_2(111)$ surface. This coverage indicates that the formic acid is reacting on a large portion of the surface and not just at isolated vacancies or step edges.

3.1.2. Soft X-ray Photoemission. The C 1s and O 1s spectra that were produced by the surface intermediates during the thermally induced decomposition of HCOOH on $CeO_2(111)$ are presented in Figures 2a and 3a, respectively. Upon exposure of 1.8 L of HCOOH onto the clean CeO_2 surface at 90 K, a broad feature is present in the C 1s spectrum with at least two peaks discernible near 290 and 289 eV. Upon heating to 200 K, the feature near 290 eV largely disappears while the peak near 289 eV becomes better defined. The disappearance of the 290 eV feature corresponds to the desorption of physisorbed HCOOH. The C 1s was largely unchanged at 250 K but gradually shifts to progressively greater binding energies at 300 and 350 K. The peak position stabilizes near 290 eV after annealing to 400 K until the C disappears after annealing to 600 K. The peak shifts between 300 and 400 K coincide with the temperature region where H_2O, CO_2, and H_2 desorb (Figure 1).

In the O 1s spectra shown in Figure 3a, a very broad contribution from HCOOH is present between 532 and 535 eV alongside the ever-present lattice oxygen feature from CeO_2 at 530.4 eV. With heating to 250 K, the intensity on the high binding energy side of the adsorbate related signal disappears and only a peak at 532.5 eV remains. As with the C 1s spectra, the disappearance of the higher binding energy feature is related to the desorption of physisorbed HCOOH. Also, in a manner

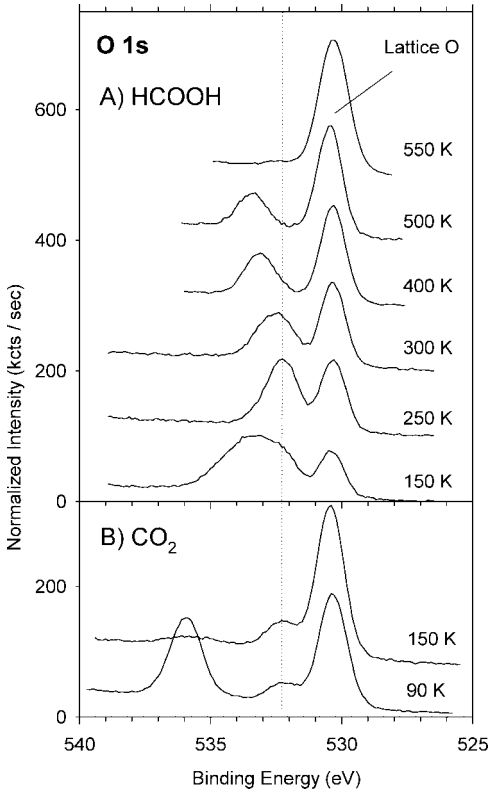

Figure 3. O 1s sXPS following (a) HCOOH and (b) CO_2 adsorption on $CeO_2(111)$ at 90 K and then annealed as indicated.

similar to the C 1s spectra, the adsorbate-related feature shifts to progressively higher binding energies as the sample was annealed from 250 to 400 K. The intensity of this feature decreases, and the intensity of the lattice O peak increases, as the sample was heated and O-containing products desorb.

3.1.3. Near-Edge X-ray Absorption. The C K-edge NEXAFS spectra for HCOOH on $CeO_2(111)$ are shown in Figure 4a. A comparison of the observed features with those cited in the literature is presented in Table 1. The top spectra in Figure 4a show the C K-edge absorption following a 2 L exposure of HCOOH at 90 K onto a clean CeO_2 surface at two different angles of incidence. Spectra at a normal angle of incidence (0°) and at a near grazing angle of incidence (65°) are depicted by solid and dotted lines, respectively. On the basis of the sXPS data (Figures 2a and 3a), at least two species contribute to the spectra at 90 K. The observed features can be assigned to either HCOOH[26] or $HCOO^-$.[27] A strong π^* C═O feature appears at 288 eV followed by weaker σ contributions at 292.0, 297.8, and 300.1 eV corresponding to σ^* C−H, σ_1^* C−O(H), and σ_2^* C═O, respectively. The polarization dependence of the π^* resonance suggests that the molecular plane is oriented away from the normal, i.e. tilted toward the surface. This is consistent with what has been observed in NEXAFS spectra of multilayer formic acid on Si(111).[28]

Upon heating to 250 K, the NEXAFS intensity decreased due to the desorption of HCOOH, leaving nominally a single species as shown in the sXPS spectra (Figures 2a and 3a). Note that in Figure 4 the spectra have been scaled for comparison so that nominal edge jump is always ca. 1. The normal angle spectrum depicts a sharp π^* C═O contribution at 287.7 eV with a very broad σ_2^* C═O feature at 300 eV. When the angle changes to near grazing, the intensity of the π^* C═O peak decreases by ca. 50%. The σ^* C−H peak shifts from 292 to 290.2 eV. Unlike at 90 K, there is a clear distinction between the σ_1^* C−O and

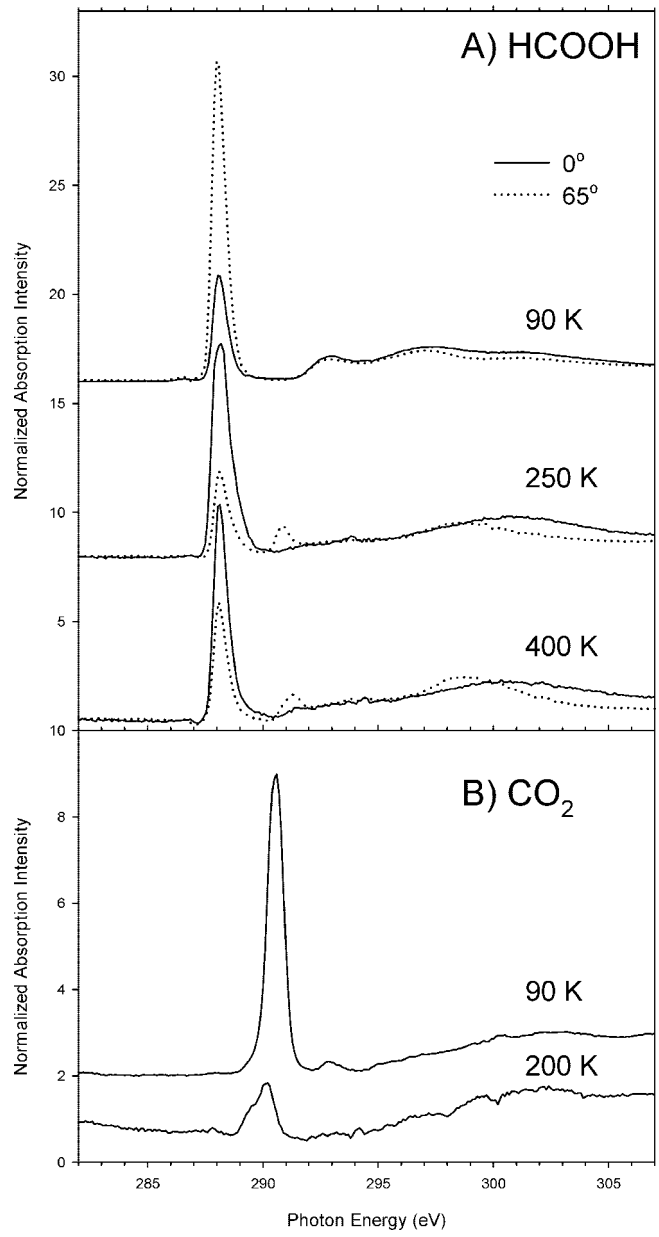

Figure 4. C K-edge NEXAFS spectra following (a) HCOOH and (b) CO_2 adsorption on $CeO_2(111)$ at 90 K and then annealed as indicated. The solid lines indicate spectra recorded at normal incidence (0°), while the dotted lines were recorded at grazing incidence (65°).

TABLE 1: C K-Edge Excitation Energies (eV) for Formic Acid (A) and Formate (B)

	π^* C═O	σ^* C−H	σ_1 *C−O	σ_2 *C═O
	A. Formic Acid			
HCOOH/CeO_2 90 K	288.0	292.0	297.8	300.0
HCOOH/Si(111) multilayer[28]	288.6	293.7	297.5	301.4
HCOOH gas phase[26]	288.2	291.8	297.1	303.0
	B. Formate			
$HCOO^-$/CeO_2 250 K	288.1	290.9	298.5	300.8
$HCOO^-$/CeO_x 300 K	287.8	290.8	299.0	300.9
$HCOO^-$/Ag(110)[27]	288.3	292.2	298.6	301.9
$HCOO^-$/Cu(110)[41]	287.9	290.4	297.6	300.4

σ_2^* C═O contributions, with the σ_1^* C−O appearing in the grazing angle at ∼298 eV. The polarization dependence indicates that the molecular plane is inclined ca. 20° from the normal.

Continued heating of the surface to 400 K produced a further decrease in intensity but no sign of any new intermediate species.

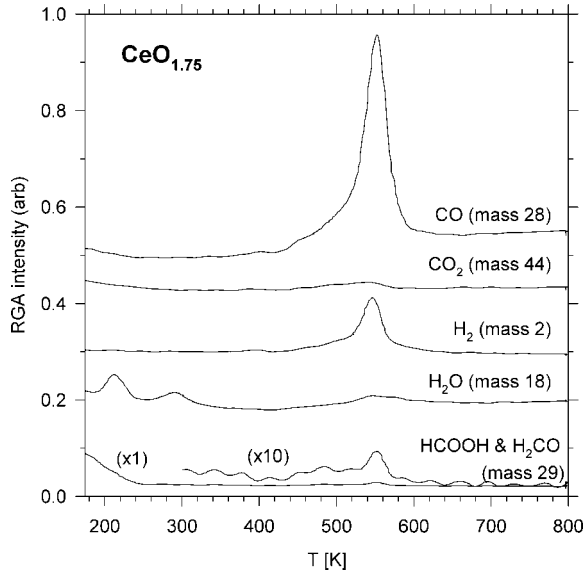

Figure 5. Temperature programmed desorption from HCOOH adsorbed on partially reduced $CeO_{1.75}$(111) at 100 K.

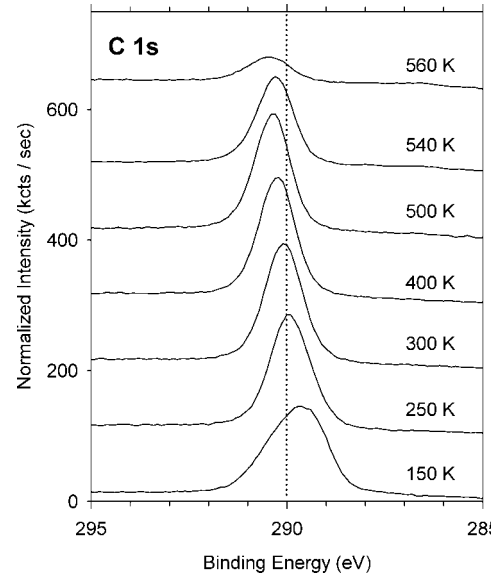

Figure 6. C 1s sXPS following of HCOOH adsorption on partially reduced $CeO_{1.75}$(111) at 90 K and then annealed as indicated.

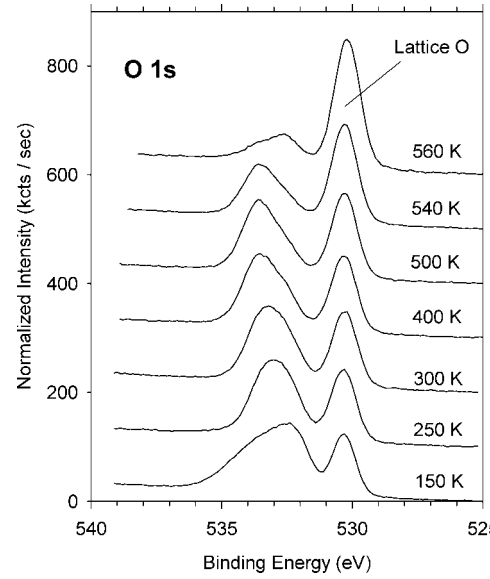

Figure 7. O 1s sXPS following of HCOOH adsorption on partially reduced $CeO_{1.75}$(111) at 90 K and then annealed as indicated.

This in contrast to the sXPS data that show a shift to higher binding energy (289.5−290 eV) (Figure 2) between 250 and 400 K.

3.2. Nonstoichiometric CeO_X Surface. ***3.2.1. Temperature Programmed Desorption.*** Figure 5 shows the TPD data from an exposure of ca. 2 L onto a reduced $CeO_{1.75}$ surface at 100 K. As on the CeO_2 surface, physisorbed HCOOH desorbed near 155 K. A shoulder extends to ca. 240 K. The most prominent C-containing decomposition product was CO, which desorbs with a sharp peak at 550 K. A leading shoulder is evident starting at about 450 K, and at higher degrees of ceria reduction, an additional feature emerges at 600 K. A trace amount of H_2CO also desorbs in this range. The formaldehyde intensity is stronger than from the fully oxidized surface (Figure 1). H_2 desorption coincides with the CO desorption. Water desorption was evident at 210, 290, and 550 K. Only a trace amount of CO_2 is evident and appears above 500 K.

The amount of CO produced was 4.0 nm^{-2} based on a comparison with HCOOH on Ru(0001). Approximately the same amount of formic acid adsorbed and reacted on the oxidized and reduced surfaces.

3.2.2. Soft X-ray Photoemission (sXPS). Figure 6 details the C 1s spectra of a 2 L exposure of HCOOH onto a reduced $CeO_{1.75}$ surface. Following adsorption at 90 K and then annealing at 150 K, the spectrum consists of a broad feature with a centroid near 289.8 eV. While the overall signal is as broad as the signal from HCOOH on CeO_2 at 150 K (Figure 2), two peaks were not clearly resolved in Figure 6. At 250 K the spectrum sharpens and the peak position is at 290 eV. The peak position progressively shifts to 290.3 eV as the sample is heated to 500 K. The greatest drop in intensity occurs above 500 K, coinciding with the desorption of CO.

The O 1s spectra (Figure 7) are similar to what was observed following HCOOH adsorption on the oxidized CeO_2(111) surface (Figure 3). In addition to the lattice O feature at 530.4 eV, a broad, adsorbate-related feature occurs at higher binding energies with apparent peaks near 532 and 533.5 eV. When the sample was annealed to 250 K, the adsorbate signal collapses into a broad, fairly symmetric peak near 533 eV. As the sample was annealed further, the signal again becomes asymmetric with the maximum near 533.5 eV and a shoulder at lower binding energies near 532.5 eV.

3.2.3. Near-Edge X-ray Absorption. The NEXAFS experiments performed with 2 L of HCOOH over reduced CeO_X are not shown in this paper because the spectra were qualitatively identical to those presented in Figure 4. The peak positions are listed in Table 1.

3.3. Evidence of Redox Reactions. Oxidation−reduction reactions between HCOOH and ceria were indicated by a change in oxidation state of the Ce and by incorporation of lattice oxygen into the desorption products. In Figure 8, Ce 3d spectra are shown for initially oxidized (a) and initially reduced (b) ceria surfaces before and after exposure and TPD of HCOOH. In each case the surfaces have been subjected to 10 exposure/TPD cycles. In Figure 8a, the surface was initially more than 90% Ce^{4+} ($CeO_{1.95}$). After 10 TPD cycles, the degree of oxidation was reduced to 80% Ce^{4+} ($CeO_{1.90}$). In Figure 8b the surface initially contained 50% Ce^{4+} ($CeO_{1.75}$). After 10 TPD cycles the Ce was oxidized to 80% Ce^{4+} ($CeO_{1.90}$).

An oxidized film was grown using $^{18}O_2$. The surface was exposed to HCOOH containing ^{16}O at 100 K. The TPD of the

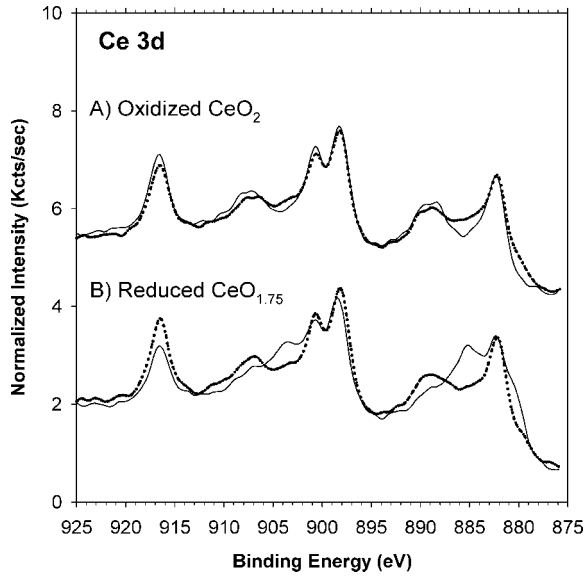

Figure 8. Ce 3d spectra before (solid lines) and after (dotted lines) 10 adsorption cycles on (a) oxidized $CeO_2(111)$ and (b) partially reduced $CeO_{1.75}(111)$.

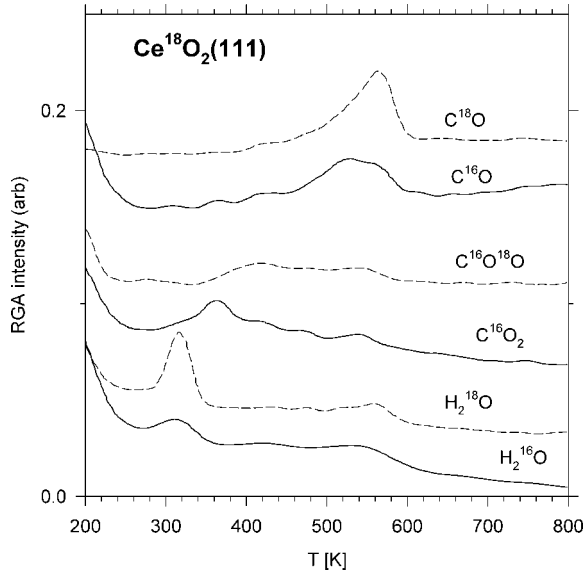

Figure 9. Temperature programmed desorption from HCOOH adsorbed on $Ce^{18}O_2(111)$ at 100 K.

O-containing desorption products is shown in Figure 9. The water that desorbs near 320 K contains predominantly ^{18}O. There is also some $H_2{}^{16}O$ at this temperature, although it is not known how much of this may have resulted from exchange in the mass spectrometer ionizer. The broad water desorption between 350 and 600 K shows equivalent amounts of $H_2{}^{16}O$ and $H_2{}^{18}O$. The isotopic mixing in the CO_2 shows two different results. The peak near 360 K shows little incorporation of ^{18}O from the substrate. Alternatively, the broader desorption from 350 to 560 K contains predominantly a single ^{18}O constituent. There was no evidence of $C^{18}O_2$. The CO desorption between 450 and 600 K shows roughly equivalent amounts of $C^{16}O$ and $C^{18}O$. However, the $C^{16}O$ desorption is skewed toward lower temperatures, whereas the $C^{18}O$ is skewed toward higher temperatures.

We note that the TPD spectra in Figure 9 are somewhat different compared to the spectra shown in Figure 1. There is less CO_2 desorption, there is less separation between the CO peaks, and all of the peaks have shifted to slightly higher temperatures. The shift from what was observed in Figure 1 to that shown in Figure 9 and ultimately to what was seen on a reduced surface in Figure 5 occurs over a very narrow range of Ce oxidation states. Although XPS was unavailable when the data in Figure 9 was collected, the spectra are consistent with what was observed from a surface with ca. 10% Ce^{3+} ($CeO_{1.95}$). Sequential TPD runs starting with an initially oxidized surface produce this progression due to the initial reduction of the $CeO_2(111)$ by formic acid. Similarly, sequential TPD runs starting with a reduced surface progress in a reverse manner as formic acid oxidizes the reduced ceria.

The reaction and desorption of HCOOH from reduced $Ce^{18}O_X$ shows nearly equal amounts of ^{18}O and ^{16}O in the CO and H_2O products at 550 K (data not shown).

4. Discussion

An interpretation of the formic acid reaction pathways on $CeO_X(111)$ in terms of dehydrogenation (reaction 2) or dehydration (reaction 3) would be an oversimplification due to the intimate participation of the ceria substrate in the reaction process. The TPD spectra (Figure 1) from fully oxidized $CeO_2(111)$ show a clear indication of dehydrogenation, as CO_2 and H_2 were produced simultaneously at 350 K. The absence of ^{18}O in the CO_2 (Figure 9) indicates that the lattice O was not incorporated into the products in this reaction. However, the water that desorbs at 300 K was predominantly $H_2{}^{18}O$. This indicates that the hydrogen in the formic acid was reacting with the O in the ceria. Rather than the simple dehydration reaction indicated in reaction 3, the more likely pathway is

$$2HCOOH(g) + 2O(l) \rightarrow 2HCOO^-(a) + 2HO(a) \rightarrow 2HCOO^-(a) + H_2O(g) + O(l) + V_O \quad (5)$$

where O(l) is lattice O and V_O is an O vacancy.

As evident in Figure 1, not all of the remaining formate ($HCOO^-$) decomposes into CO_2 and H_2 at 350 K. The CO desorption at higher temperatures is indicative of dehydration, as shown in reaction 3. Some water desorption accompanies the CO desorption, but the magnitude does not appear to balance the amount of CO produced. Rather than producing water, some of the $HCOO^-$ may be reacting with the lattice vacancies to reoxidize the substrate:

$$HCOO^-(a) + V_O \rightarrow CO(g) + \frac{1}{2}H_2(g) + O(l) \quad (6)$$

As indicated by the Ce 3d spectra (Figure 8), the balance of the various reactions produces a net reduction of the ceria surface.

Stubenrauch et al. reported only formate decomposition near 600 K on single crystal $CeO_2(111)$, and this decomposition followed predominantly the dehydration pathway (reaction 3) with a smaller amount of dehydrogenation.[17] They did not see CO_2, H_2, or water produced at lower temperatures, nor did they report any evidence of the involvement of substrate O in the reaction pathway. It is not clear why the current results differ from this earlier result. Differences in the reactivity of methanol with $CeO_2(111)$ thin films[19] and single crystal $CeO_2(111)$[29] were also previously observed. Perhaps there are some as yet unidentified differences between the bulk crystal and the thin film.

The reaction pathway on a reduced surface is somewhat more simplified. As seen following the adsorption of water[21] and methanol,[19] surface OH is much more stable on reduced ceria compared to oxidized ceria and decomposes to form H_2 above

500 K. The reaction with formic acid on reduced ceria can be described by

$$HCOOH(g) + V_O + O(l) \rightarrow HCOO^-(a) + HO(a) \rightarrow CO(g) + H_2(g) + 2O(l) \quad (7)$$

This is the predominant pathway; however, there were small amounts of H_2O and H_2CO formed as well.

The reaction pathways observed on the structurally analogous $UO_2(111)$ surface[18] demonstrate both similarities and differences compared to those occurring on $CeO_2(111)$. Chong and Idriss propose the formation of surface formate followed by the desorption of lattice oxygen in water on $UO_2(111)$. This is similar to what is observed on $CeO_2(111)$, as shown in reaction 5. These formates then proceed to decompose through dehydration (reaction 3). This is also similar to what is observed on $CeO_2(111)$, except that reoxidation of the ceria is observed instead of water formation (reaction 6). There is no indication that the formates reoxidize the partially reduced UO_X. Further, on sputtered UO_X, the adsorbed formates undergo primarily dehydrogenation (reaction 2), again demonstrating a lack of reoxidation of the reduced UO_X. The main difference between $CeO_2(111)$ and $UO_2(111)$ appears to be the ability of the substrate to participate in redox reactions with the adsorbate, i.e. UO_2 is not as good of an oxygen storage material as CeO_2. The chemical differences outweigh the structural similarities.

The sXPS and NEXAFS spectra identify the surface intermediates that were formed on $CeO_2(111)$ and provide additional clues as to why one pathway is preferred over another. The TPD spectra from oxidized CeO_2 (Figure 1) show a large amount of water and H_2 desorption below 400 K and considerable CO desorption above 400 K. This suggests that a H-deficient species such as CO_3^{2-} may be the dominant surface species at high temperature.

A complementary study of the adsorption CO_2 on $CeO_2(111)$ was performed in order to distinguish between a carbonate and a formate species. Identification based solely on sXPS data is challenging. This fact is demonstrated in Figure 2b following the adsorption of CO_2 onto $CeO_2(111)$ at 90 K. A large feature corresponding to weakly bound CO_2 is observed at 292 eV accompanied by a smaller CO_3^{2-} feature at ~290 eV. Desorption of the weakly bound component upon heating to 150 K leaves only the carbonate feature. Its peak position is similar to that produced by HCOOH on $CeO_2(111)$ after it is annealed to 400 K. However, the O 1s spectra (Figure 3) demonstrate a clear distinction between the species formed by HCOOH and CO_2. At 250 K, the HCOOH intermediate has a peak position that is similar to that of the strongly bound CO_2 intermediate (532.3 eV). However, as the sample is annealed the HCOOH intermediate shifts to 533.8 eV, away from the position of the strongly bound CO_2-derived species. This suggests that HCOOH does not form a dehydrogenated CO_3^{2-} species.

The C K-edge NEXAFS (Figure 4a) provides the definitive identification of the HCOOH-derived surface species. The spectra are only consistent with HCOOH or $HCOO^-$. The intense π^* resonance is at 288 eV and the σ^* resonances are at 292/290, 298, and 300.5 eV. These positions are consistent with the values reported in the literature for HCOOH and $HCOO^-$.[26] The π^* resonance following CO_2 adsorption is at 290.5 eV[30] (Figure 4b). This is consistent with the peak position reported for CO_3^{2-} on various surfaces.[23]

The variations in the peak positions for $HCOO^-$ in the C 1s and O 1s spectra are analogous to what was observed for methoxy on $CeO_2(111)$.[19] It was hypothesized that the change in the methoxy peak positions was associated with a change in the adsorption site. The fully oxidized $CeO_2(111)$ surface has relatively few O vacancies,[22] so the only available adsorption site is presumably atop a Ce cation. However, as the surface is annealed, water desorbs, producing O vacancies. It is also possible that exchange occurs between methoxy/formate and OH, thus exchanging adsorption sites. The increase in binding energy would be indicative of a shift from a low coordinated adsorption site atop a single Ce cation to a higher coordination site in an O vacancy amidst three Ce cations. A similar correlation between adsorption site and binding energy has been identified for adsorbates on metal surfaces[31,32] and for S on $CeO_X(111)$.[33]

Different formate adsorption sites would help explain the low- and high-temperature decomposition pathways on $CeO_2(111)$. At 350 K, the formate produces CO_2 and H_2. The Ce−O bond in the low coordinated top site is presumably weaker than the bond in the 3-fold hollow site; hence, there is less of a driving force to break the C−O bond. The incorporation of ^{18}O from the $Ce^{18}O_2(111)$ surface (Figure 9) is also consistent with adsorption in a top site leading to decomposition at 350 K and adsorption in a hollow site decomposing at higher temperatures. If the formate were bound in a hollow site, one might expect the C atom to break one bond with an O in a hollow site and make a new bond with an O in a neighboring hollow site, thus exchanging O between the parent formate and the surface. There is little incorporation of ^{18}O in the CO_2 at 350 K but roughly an equal amount of ^{18}O and ^{16}O in the CO_2 and CO that desorbs above 400 K.

The C 1s and O 1s spectra observed following HCOOH adsorption and reaction on reduced $CeO_X(111)$ (Figures 6 and 7) are consistent with interpreting the changes in binding energies with changes in adsorption site. The binding energies are initially greater, and the shifts with temperature smaller, than what is observed on oxidized $CeO_2(111)$. This is because higher coordination sites are available upon adsorption. Some shifting still occurs because some water still desorbs from the partially reduced surface (Figure 5) and site exchange with OH may also occur. The O 1s spectra are complicated by the presence of both $HCOO^-$ and OH at higher temperatures. The asymmetry in the O 1s adsorbate related features and the peak clearly resolvable at 532.8 eV at 560 K are likely due to OH.[21]

The most perplexing observation in the current study is the lack of H-containing desorption products above 400 K from $CeO_2(111)$ (Figure 1). Although some of the H is contained in the small amounts of H_2, H_2O, and H_2CO observed, much of the H is unaccounted for. This is not an instrumental artifact, since the reaction of methanol[34] or formic acid[25] with the clean Ru(0001) substrate reproduced the TPD results reported in the literature. The most likely explanation is diffusion of the H into the ceria substrate. This phenomenon appears to be the most significant on the oxidized surface, since H_2 desorption is clearly evident at elevated temperatures from the reduced surface (Figure 5). Similar behavior was observed following methanol adsorption and decomposition. Methoxy is the only C-containing species on oxidized $CeO_2(111)$. However, H_2CO is the predominant desorption product at elevated temperatures, with only a small amount of H_2O and CH_3OH formed. Some of the methyl hydrogen is lost in a manner similar to the decomposition of formate.

While surface formate is clearly indicated as the only C-containing surface species, the adsorption geometry is less certain. Three possible adsorption geometries are depicted below. On fully oxidized $CeO_2(111)$, the monodentate configuration (I) would appear to be the most likely. Crowding by

surface oxygen atoms seemingly would inhibit the two O atoms in the formate from bridging between two Ce atoms in a bridging bidentate configuration (II) or from bonding to a single Ce atom in a chelating bidentate configuration (III). Further, the chelating structure is also unlikely because, on $CeO_2(111)$, the top layer of Ce only has one coordination vacancy and bonding to two O atoms would increase the coordination to nine. On the reduced $CeO_X(111)$ surface, there are O vacancies, so the Ce atoms have lower initial coordination and crowding by surface O is less likely to be important.

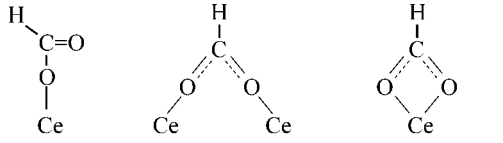

(I) Mono-dentate (II) Bridging bi-dentate (III) Chelating bi-dentate

Stubenrauch et al.[17] have argued that the spacing between Ce^{4+} ions on the (111) surface (0.383 nm) is too wide to allow the formate O to adsorb on two separate Ce^{4+} cations (II), since the O−O distance in sodium acetate is only 0.22 nm. However, bridging configurations have been proposed on $TiO_2(110)$ between Ti atoms separated by 0.325 nm,[15] and bridging carboxylate structures have been determined in organometallic complexes between metal centers separated by 0.356 nm.[35] Therefore, the distance between the metal centers is not a simple predictor of whether bridging might occur.

NEXAFS spectra show virtually no difference between the formates present at 250 and 400 K on $CeO_2(111)$. The NEXAFS from formates on CeO_2 also look the same as those on reduced $CeO_X(111)$. Stevens et al. have argued that it is not possible to differentiate between monodentate and bidentate configurations based on the NEXAFS spectra.[27] However, Schertel et al. have suggested that, if the position of the π^* resonance for the carboxylate is the same as that of the multilayer carboxylic acid, the carboxylate is bound as a bidentate.[36] If the π^* resonance is shifted to lower energy, the carboxylate is monodentate. By this reasoning all of the formates on the ceria films in this study should be bidentate (configuration II or III), since the π^* resonance does not shift and is same as for the multilayer formic acid.

Vibrational spectroscopy might provide an indication of the bonding configuration. The difference in frequency between the ν_a(OCO) and ν_s(OCO) modes for adsorbed formate has been used to differentiate between the monodentate and the bidentate configurations. A large difference in the frequencies has been associated with a monodentate species, and a small difference in frequency has been associated with a bidentate species. Stubenrauch et al. found a value of 220 cm^{-1} for formates on $CeO_2(111)$ and concluded that the species was monodentate.[17] However, Li et al. studied formic acid adsorption on high surface area ceria powders and assigned species with a frequency difference of ca. 350 cm^{-1} to a monodentate and species with a frequency difference of ca. 200−250 cm^{-1} to bidentate species.[37] Likewise, Siokou and Nix identified monodentate (316 cm^{-1}) and bidentate (238 cm^{-1}) formate species on thin $CeO_2(111)$ grown on Cu(111).[38]

Experiments are currently underway to compare the vibrational spectra of formates on $CeO_X(111)$ at different temperatures on surfaces with different degrees of reduction. These results will be correlated with the present TPD, sXPS, and NEXAFS data in order to determine which configurations are present. Theoretical calculations, as have been conducted for methanol[39] and formaldehyde[40] on $CeO_2(111)$, are also being conducted to determine which formate structures are the most stable.

5.Conclusion

Formic acid adsorbs on both fully oxidized and partially reduced $CeO_X(111)$ surfaces. Above 200 K, the only C-containing surface species is formate, $HCOO^-$. On oxidized $CeO_2(111)$, surface hydroxyls react at 300 K to form water. The remaining formates decompose in two different channels. H_2 and CO_2 are formed at 350 K and predominantly CO is produced above 400 K. It is hypothesized that H diffuses into the ceria. On reduced $CeO_X(111)$, the formate only decomposes through the higher temperature, CO-producing channel. H_2 is also produced from the formate decomposition as well as from the surface hydroxyls. Evidence suggests that formate adsorbed in a low coordination site atop a Ce cation leads to the low-temperature decomposition, while formate adsorbed in higher coordination O vacancy sites leads to higher-temperature decomposition.

Acknowledgment. S.D.S. would like to thank the efforts of Dennis Potshka (NSLS). Research was sponsored by the Division of Chemical Sciences, Geosciences, and Biosciences, Office of Basic Energy Sciences, U.S. Department of Energy, under contract DE-AC05-00OR22725 with Oak Ridge National Laboratory, managed and operated by UT-Battelle, LLC. Use of the National Synchrotron Light Source, Brookhaven National Laboratory, was supported by the U.S. Department of Energy, Office of Science, Office of Basic Energy Sciences, under Contract No. DE-AC02-98CH10886.

References and Notes

(1) Spencer, M. S. *Catal. Lett.* **1995**, *32*, 9.
(2) *Catalysis by Ceria and Related Materials*; Trovarelli, A., Ed.; Imperial College Press: London, 2002.
(3) Pettigrew, D. J.; Trimm, D. L.; Cant, N. W. *Catal. Lett.* **1994**, *28*, 313.
(4) Jacobs, G.; Patterson, P. M.; Graham, U. M.; Crawford, A. C.; Davis, B. H. *Int. J. Hydrogen Energy* **2005**, *30*, 1265.
(5) Jacobs, G.; Ricote, S.; Graham, U. M.; Patterson, P. M.; Davis, B. H. *Catal. Today* **2005**, *106*, 259.
(6) Sakurai, H.; Akita, T.; Tsubota, S.; Kiuchi, M.; Haruta, M. *Appl. Catal., A* **2005**, *291*, 179.
(7) Ritter, S. K. *Chem. Eng. News* **2007**, *85*, 11.
(8) Barteau, M. A. *Chem. Rev.* **1996**, *96*, 1413.
(9) Kim, K. S.; Barteau, M. A. *Langmuir* **1990**, *6*, 1485.
(10) Kim, K. S.; Barteau, M. A. *J. Catal.* **1990**, *125*, 353.
(11) Libby, M. C.; Watson, P. C.; Barteau, M. A. *Ind. Eng. Chem. Res.* **1994**, *33*, 2904.
(12) Idriss, H.; Lusvardi, V. S.; Barteau, M. A. *Surf. Sci.* **1996**, *348*, 39.
(13) Diebold, U. *Surf. Sci. Rep.* **2003**, *48*, 53.
(14) Gutierrez-Sosa, A.; Evans, T. M.; Woodhead, A. P.; Lindsay, R.; Muryn, C. A.; Thornton, G.; Yoshihara, J.; Parker, S. C.; Campbell, C. T.; Oldman, R. J. *Surf. Sci.* **2001**, *477*, 1.
(15) Hayden, B. E.; King, A.; Newton, M. A. *J. Phys. Chem. B* **1999**, *103*, 203.
(16) Yoshihara, J.; Campbell, C. T. *Surf. Sci.* **1998**, *407*, 256.
(17) Stubenrauch, J.; Brosha, E.; Vohs, J. M. *Catal. Today* **1996**, *28*, 431.
(18) Chong, S. V.; Idriss, H. *Surf. Sci.* **2002**, *504*, 145.
(19) Mullins, D. R.; Robbins, M. D.; Zhou, J. *Surf. Sci.* **2006**, *600*, 1547.
(20) Zhou, J.; Mullins, D. R. *Surf. Sci.* **2006**, *600*, 1540.
(21) Kundakovic, L.; Mullins, D. R.; Overbury, S. H. *Surf. Sci.* **2000**, *457*, 51.
(22) Mullins, D. R.; Radulovic, P. V.; Overbury, S. H. *Surf. Sci.* **1999**, *429*, 186.
(23) Stohr, J. *NEXAFS Spectroscopy*; Springer-Verlag: New York, 2003; Vol. 25.
(24) Kaindl, G.; Kalkowski, G.; Brewer, W. D.; Perscheid, B.; Holtzberg, F. *J. Appl. Phys.* **1984**, *55*, 1910.
(25) Sun, Y. K.; Weinberg, W. H. *J. Chem. Phys.* **1991**, *94*, 4587.

(26) Ishii, I.; Hitchcock, A. P. *J. Electron Spectrosc. Relat. Phenom.* **1988**, *46*, 55.
(27) Stevens, P. A.; Madix, R. J.; Stohr, J. *Surf. Sci.* **1990**, *230*, 1.
(28) Outka, D. A.; Stohr, J.; Madix, R. J.; Rotermund, H. H.; Hermsmeier, B.; Solomon, J. *Surf. Sci.* **1987**, *185*, 53.
(29) Ferrizz, R. M.; Wong, G. S.; Egami, T.; Vohs, J. M. *Langmuir* **2001**, *17*, 2464.
(30) Gutierrez-Sosa, A.; Evans, T. M.; Parker, S. C.; Campbell, C. T.; Thornton, G. *Surf. Sci.* **2002**, *497*, 239.
(31) Mullins, D. R.; Huntley, D. R.; Tang, T.; Saldin, D. K.; Tysoe, W. T. *Surf. Sci.* **1997**, *380*, 468.
(32) Mullins, D. R.; Lyman, P. F.; Overbury, S. H. *Surf. Sci.* **1992**, *277*, 64.
(33) Mullins, D. R.; McDonald, T. S. *Surf. Sci.* **2007**, *601*, 4931.
(34) Hrbek, J.; Depaola, R. A.; Hoffmann, F. M. *J. Chem. Phys.* **1984**, *81*, 2818.
(35) Rzaczynska, Z.; Mrozek, R.; Glowiak, T. *J. Chem. Crystallogr.* **1997**, *27*, 417.
(36) Schertel, A.; Woll, C.; Grunze, M. *J. Phys. IV* **1997**, *7*, 537.
(37) Li, C.; Domen, K.; Maruya, K.; Onishi, T. *J. Catal.* **1990**, *125*, 445.
(38) Siokou, A.; Nix, R. M. *J. Phys. Chem. B* **1999**, *103*, 6984.
(39) Beste, A.; Mullins, D. R.; Overbury, S. H.; Harrisison, R. J. *Surf. Sci.* **2008**, *602*, 162.
(40) Donghai, M.; Deskins, N. A.; Dupuis, M. *Surf. Sci.* **2007**, *601*, 4993.
(41) Somers, J.; Robinson, A. W.; Lindner, T.; Ricken, D.; Bradshaw, A. M. *Phys. Rev. B* **1989**, *40*, 2053.

JP8016425